ELSEVIER

Journal of Photochemistry and Photobiology A: Chemistry 94 (1996) 173–189

Journal of PHOTOCHEMISTRY AND PHOTOBIOLOGY A: CHEMISTRY

Photocatalytic reactors
II. Quantum efficiencies allowing for scattering effects. An experimental approximation

Carlos A. Martín [1], Miguel A. Baltanás [2], Alberto E. Cassano [2,*]

Instituto de Desarrollo Tecnológico para la Industria Química, Universidad Nacional del Litoral and Consejo Nacional de Investigaciones Científicas y Técnicas, Güemes 3450, (3000) Santa Fe, Argentina

Received 21 June 1995; accepted 11 September 1995

Abstract

A combination of reactor modeling and specially designed experiments has been used to compute quantum efficiencies in a photocatalytic reactor. The method was applied to the photocatalytic decomposition of very low concentrations of chloroform in water solution. Titanium dioxide particles suspended in the reactor were used as the photocatalyst.

The photocatalytic reaction was carried out in a fully irradiated photoreactor (FIP reactor) to make sure that all the catalyst mass existing in the reactor was photoactivated. Polychromatic radiation was employed. Radiation and mass balances applied to the reactor while using a homogeneous actinometric solution permitted computation of the incident radiation at its boundaries. This boundary condition was then used to solve the radiative transfer equation inside the heterogeneous reactor.

With this approach the local volumetric rate of energy absorption inside the photocatalytic reactor can be calculated with a good degree of approximation. After integration for the whole reactor, the volume average radiation absorption rate was obtained and then used to calculate quantum efficiencies at initial conditions.

With the proposed method, quantum efficiencies can be computed with good confidence. For the chloroform decomposition in particular, under the investigated experimental conditions, it was found that the quantum efficiency: (i) increases when the initial concentration of substrate is augmented, (ii) is almost insensitive to the initial concentration of dissolved oxygen and (iii) increases at lower levels of the volume-averaged absorbed radiation. This last result seems to be typical of photoreacting devices where the levels of incident radiation are moderate.

Keywords: Photocatalytic reactors; Quantum efficiencies; Absorption and scattering effects; Titanium dioxide; Chloroform decomposition

1. Introduction

For many centuries, natural purification of polluted water streams has been caused by sunlight initiated redox reactions involving organic compounds that finally break down to carbon dioxide and other normally innocuous products. Additionally, it has been known for many years now that this process can be emulated and even improved by interaction of the UVB part of the solar spectrum with some widespread, rather inexpensive semiconductors which act as photocatalysts [1]. One of the systems most widely studied has been the light activated titanium dioxide, for the heterogeneous photocatalysed mineralization of air and water pollutants [2–12]. Thus, it has been shown beyond doubt that irradiated titanium dioxide (with light of the appropriate wavelength) provides a very attractive method for oxidizing a very wide variety of organic compounds.

Absorption of a photon by a semiconductor such as titanium dioxide leads to the generation of an electron/hole pair which can either recombine or undergo subsequent redox reactions. For example, in the presence of molecular oxygen the electron can be scavenged and the remaining hole can then produce, either directly or indirectly, the oxidation of the pollutant. No matter what the pathway is, the initiation reaction is some sort of photochemical act that depends upon the photon absorption rate.

In performing kinetic modeling, one of the key problems is the correct evaluation of the absorbed radiation inside the

* Corresponding author.

[1] Research Assistant (CONICET and U.N.L.).

[2] Professor (U.N.L.) and Research Staff Member (CONICET).

SSDI 1010-6030(95)04208-3

heterogeneous reactor as well as its proper application to obtain meaningful numerical values of relevant kinetic information, as it is the case of quantum yields [13–16].

The radiative transport equation applied to homogeneous chemically reacting systems where only radiation absorption occurs, i.e. with no scattering, is a relatively simple differential equation [17–19]. However, in heterogeneous reactors, absorption and scattering effects are combined and then the radiative transfer equation has an integro-differential nature [18,20,21]. Moreover, the relevant properties required to solve this equation (i.e., the absorption and scattering coefficients and the phase function) are very difficult to measure.

This paper addresses some of the aspects related to the measurements of the local volumetric rate of energy absorption (LVREA) in a heterogeneous reacting system made up of solid catalytic particles suspended in an oxygen-saturated, low-concentration aqueous solution of a non-absorbing pollutant. For this purpose, it is shown that a rather simple experimental device can be used which, combined with reactor analysis and very simple radiative transfer concepts, is suitable for providing a good first approximation to the actual value of the LVREA. These results are then used to calculate initial quantum efficiencies of the photodecomposition reaction employing polychromatic radiation. To illustrate matters, the mineralization of a Priority Pollutant, chloroform, using powdered titanium dioxide as the photocatalyst, has been chosen as a model system.

2. Proposed approach

As indicated by Ozisik [22] and Santarelli [23] radiative transport in participating and reacting media along a given direction of propagation of photons is described according to:

$$\frac{dI_{\underline{\Omega},\nu}(s,t)}{ds} + [\kappa_\nu(s,t)]I_{\underline{\Omega},\nu}(s,t) + [\sigma_\nu(s,t)]I_{\underline{\Omega},\nu}(s,t)$$
$$\text{absorption} \qquad \text{scattering-out}$$

$$= j^e_\nu(s,t) + \frac{1}{4\pi}\sigma_\nu(s,t)\int_{\Omega'=4\pi} p(\underline{\Omega}' \longrightarrow \underline{\Omega})I_{\underline{\Omega}',\nu}(s,t)d\Omega'$$
$$\text{emission} \qquad \text{scattering-in} \qquad (1)$$

In Eq. (1) $I_{\underline{\Omega},\nu}$ is the Spectral (monochromatic) Specific Intensity of radiation having a frequency ν (between ν and $\nu+d\nu$) and a direction of propagation characterized by the unit vector $\underline{\Omega}$, at location s in space at time t. κ_ν is the spectral volumetric absorption coefficient, σ_ν is the spectral volumetric scattering coefficient and p is the phase function (photon scattering distribution function). Integration of this partial-integro-differential equation requires a minimum of one boundary condition at the point of radiation entrance to the reactor volume. In theory it should be provided by the lamp emission properties and the characteristics, dimensions and geometry of the reacting system [21]. Its evaluation with an experimental approximation will be treated further ahead.

Usually, radiation may be arriving at one pont inside a photochemical reactor from all directions $\underline{\Omega}$ in space. For a photochemical reaction to occur, this radiation must be absorbed by an elementary reacting volume (a material point located at position $\underline{r}$ in space); thus, pencils of radiation coming from all directions (all solid angles Ω about the directions $\underline{\Omega}$) must cross the whole elementary surface that bounds such an element of volume. Hence, the relevant photochemical properties are the spectral incident radiation and the spectral radiative flux, given by:

$$G_\nu(\underline{r},t) = \int_\Omega I_\nu(\underline{r},\underline{\Omega},t)\, d\Omega \qquad (2a)$$

$$\underline{q}^{Rad}_\nu(\underline{r},t) = \int_\Omega I_\nu(\underline{r},\underline{\Omega},t)\underline{\Omega}\, d\Omega \qquad (2b)$$

In Eqs. (2a) and (2b) an integration over the solid angle Ω, for all possible directions ($\underline{\Omega}$) proceeding from the entire spherical space has been effected. For polychromatic radiation an integration over the frequency range of interest must also be performed (to account for the overlapping frequency regions where: (i) significant emission by the lamp, (ii) efficient transmission by the reactor wall and (iii) prominent absorption of radiation by the radiation absorbing species coexist):

$$G(\underline{r},t) = \int_{\nu_1}^{\nu_2}\int_\Omega I_\nu(\underline{r},\underline{\Omega},t)\, d\Omega\, d\nu \qquad (3)$$

For example, with titanium dioxide water suspensions inside a reactor made of Pyrex glass this frequency interval, in terms of wavelengths, extends from about 280 nm to about 380–390 nm. Depending upon the lamp emission characteristics, this range could be reduced even more.

In the elementary reacting volume, for a single photon absorption, energy is absorbed according to:

$$e^a_\nu(\underline{r},t) = \kappa_\nu(\underline{r},t)G_\nu(\underline{r},t) \qquad (4)$$

where e^a_ν is the spectral local volumetric rate of energy absorption (LVREA). For polychromatic radiation:

$$e^a(\underline{r},t) = \int_{\nu_1}^{\nu_2}\int_\Omega \kappa_\nu I_\nu(\underline{r},\underline{\Omega},t)\, d\Omega\, d\nu \qquad (5)$$

The final, linking step consists in writing the photochemical (or photoelectrochemical) local initiation rate, which is always some function of e^a. Its form depends on the reaction mechanism. The reaction rate and the LVREA result a function of the three spatial coordinates ($\underline{r}$) and perhaps the time t. Thus, Eq. (5) gives local values of the absorbed energy. Even in a perfectly mixed reactor, owing to the existence of absorption, scattering and geometrical effects $e^a(\underline{r},t)$ is non uniform in space. To obtain a global value of the reaction rate (to be compared with the observable one) an integration over

the reactor volume will be always required. If concentrations and temperature are uniform, the averaging procedure may be restricted to the LVREA. In any event, for quantum yields or quantum efficiencies determinations only the VREA (volume averaged value of the LVREA) is needed:

$$\langle e^a(t)\rangle_{\text{Reactor volume}} = \frac{\int_{\text{Vol.}} e^a(\underline{r},t)\,\mathrm{dV}}{\int_{\text{Vol.}} \mathrm{dV}} \qquad (6)$$

To be useful for reactor design, reaction rates must be ultimately known as an intensive quantity and therefore expressed per unit reaction volume (alternatively, in a surface reaction, per unit surface area); in our case, we will be interested in the irradiated volume (or irradiated catalyst area). One of the requisites to produce meaningful numerical kinetic values is to make sure that the reactor volume is very well defined; in our case this condition must be translated into a system where the whole reactor volume receives radiation. With this idea in mind we developed the concept of a fully irradiated photoreactor (FIP reactor). This is a reactor in which every catalytic particle "sees" photons. The optical density of the reacting medium is the key parameter, which means that the reactor size and the catalyst concentration must be careful and jointly chosen.

As indicated before, scattering-in gives to the radiative transfer equation (RTE) an integro-differential mathematical nature that makes it difficult to solve. The trouble with its correct use is not only due to its mathematical complexities: besides, its solution requires the exact knowledge of the phase function p, which turns out to be an even more complex problem. For more details, the interested reader can resort to Cabrera et al. [24,25]. However, it can be readily seen that if scattering-in could be neglected, the RTE would take on a form similar to the classical Lambertian exponential decay usually observed in homogeneous systems and the phase function would not be required. Indeed, this is a very attractive approximation.

This simplification is equivalent to the assumption of single scattering that may be better approached when the particle concentration is very small, the particle radiation absorption is high and the reactor characteristic optical length is very small. Some of these conditions must also be fulfilled to obtain a FIP reactor.

A theoretical criterion for neglecting multiple scattering is given by Siegel and Howell [26]. For our case it can be translated into an expression of the form $\sigma\Delta s < 0.1$, although strong absorption can turn this condition less stringent. As it will be seen in what follows, this limit condition (for a safe a priori application of the assumption) is not quite fulfilled in our case. Thus, the validity of the proposed approximation will finally rest on an experimental verification.

The goodness of the FIP reactor condition and the single scattering approximation can be experimentally tested in a rather simple reactor. The system will be described in what follows. Furthermore, it will be shown how the same concepts can be used to measure the boundary condition required by Eq. (1).

3. Experimental set up concept

An almost trivial solution to the above stated problems can be obtained by means of three concentric, cylindrical (two of them annular) reactors, as it is shown in Fig. 1.

Let us think of a reactor fully irradiated in a uniform manner from the outside. This reactor can be portrayed by the one described in Fig. 1, placed in one of the focal axes of a cylindrical reflector of elliptical cross section [27]. A tubular lamp can be located at the other focal axis (Fig. 2). The elliptical reflector concentrates the radiation energy coming out of the lamp into the reactor external boundaries. When some restrictions in the geometrical arrangement of the equipment are fulfilled, the irradiation from outside is almost uniform [28].

Water coming form a thermostatic bath circulates through the external annular space (III, in Fig. 1). It is used to keep the reaction temperature constant and, particularly, to absorb the infrared radiation produced by the lamp. The intermediate annular space (II) can be used to circulate a homogeneous actinometric solution (A2) or different solid concentrations (j) of the photocatalytic suspension [Ti(j)]. In the first case, with the aid of a simple radiation model, an experimental

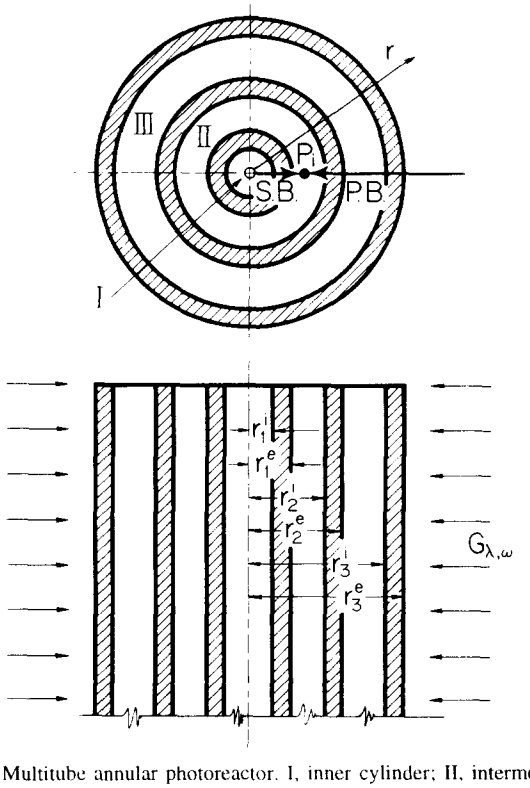

Fig. 1. Multitube annular photoreactor. I, inner cylinder; II, intermediate annular space; III, external annular space (infrared filter/thermostatic solution); P.B.: primary beam, S.B.: secondary beam, $G_{\lambda,\omega}$: incident radiation (boundary condition).

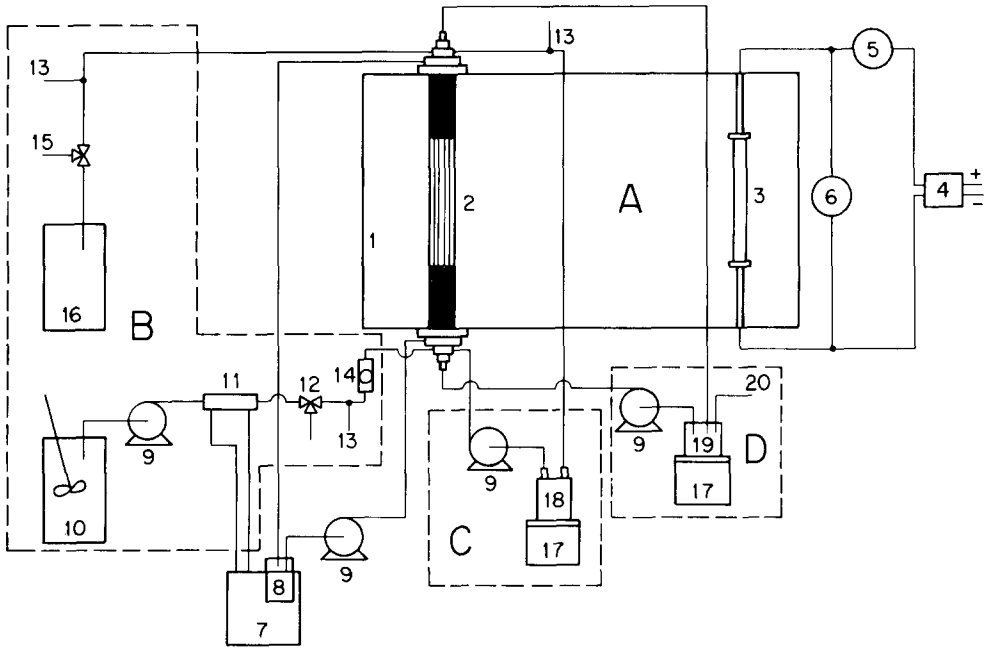

Fig. 2. Experimental set-up. (A) General purpose units: (1) Cylindrical reflector of elliptical cross section, (2) photoreactor, (3) lamp, (4) lamp ballast, (5) ammeter, (6) voltmeter, (7) thermostatic bath, (8) infrared filter, (9) peristaltic pump. (B) Actinometer equipment (section II): (10) actinometer tank (inlet), (11) heat exchanger, (12) sampling port (inlet), (13) thermometer, (14) flowmeter, (15) sampling port (outlet), (16) actinometer tank (outlet). (C) Photocatalytic reaction: (17) magnetic stirrer, (18) titania suspension tank (V_T^{II}). (D) Actinometer equipment (section I): (19) actinometer tank (V_T^{I}), (20) sampling port.

value of the boundary condition at $r=r_3^e$ and also at $r=r_2^i$ required for the photocatalytic reactor model (see next section) can be obtained; alternatively, when a solid suspension circulates through Section II, the annular space is used as a photocatalytic reactor. In the latter case, if the annular space ($r_2^i - r_1^e$) operates as a FIP system, some radiation will come out through its inner walls ($r=r_1^e$) as well. A second actinometric solution (A1) circulates inside the inner cylinder (I). It serves three different purposes: (i) to make sure that a measurable amount of radiation comes out of the reactor II (at $r=r_1^e$) when it is used with the solid suspension, thus ensuring its FIP operation, (ii) to absorb the outgoing radiation from $r=r_1^e$ to prevent its entrance into the reactor II through the opposite side, and (iii) to verify predictions of the outgoing radiation from reactor II (at $r=r_1^e$) by measuring the absorbed radiation (entering at $r=r_1^i$) that makes the actinometer circulating inside the inner cylinder I react. These predictions at $r=r_1^e$ can be obtained from the radiation model employed in the photocatalytic system, thus verifying, for example, the plausibility of the single scattering approximation.

For actinometries, the homogeneous decomposition of the uranyl oxalate complex will be used. More details on materials and methods will be given in the specific section of this report.

4. Modeling of the systems

Isothermal conditions will always be ensured. In both, the actinometric and the photocatalytic reactions, the reactant disappearance will be followed. So, the radiative transport equation and the mass balance of just one species are required.

4.1. Radiative transfer equation

The following assumptions are made: (i) no radiation emission inside the reactor, (ii) scattering-in is not very important (to be tested experimentally) and (iii) optical properties are independent of position and time. Then, Eq. (1) expressed in terms of wavelengths reduces to:

$$\frac{dI_\lambda(s,\underline{\Omega})}{ds} = -(\kappa_\lambda+\sigma_\lambda)I_\lambda(s,\underline{\Omega}) \tag{7}$$

Since $dI/ds=\underline{\Omega}\cdot\underline{\nabla}I=\underline{\nabla}\cdot(\underline{\Omega}I)$, multiplying by $d\Omega$, integrating over $\Omega=4\pi$ and recalling Eqs. (2a) and (2b), one gets:

$$\underline{\nabla}\cdot\underline{q}_\lambda^{Rad} = -\beta_\lambda G_\lambda(\underline{r}) \tag{8}$$

where $\beta_\lambda=\kappa_\lambda+\sigma_\lambda$ (in a homogeneous medium $\beta_\lambda=\kappa_\lambda$).

At this point, considering the small radial distances involved in the experimental set-up (see section 5) and that the boundary condition will be obtained from experiments, an additional simplification is made: incidence and radiation transport inside the reactor can be adequately represented by the radial model [19,29]. This means that $I_\lambda(\underline{r})=I_\lambda(r)$ only. Eq. (8) can be written in a cylindrical coordinate system and, for this model, the θ and z components of the vector $\underline{q}_\lambda^{Rad}(\underline{r})$ are nonexistent. Moreover, in this case, $q_{\lambda,r}^{Rad}(r)\equiv G_\lambda(r)$ and the final result is:

$$\frac{1}{r}\frac{d}{dr}[rG_\lambda(r)] = -\beta_\lambda G_\lambda(r) \quad (9)$$

This equation can be applied to any of the annular spaces (reactor walls made of Pyrex glass, refrigerating water in section III, homogeneous actinometer or solid catalytic suspension in section II), and to the inner cylinder (homogeneous actinometer in section I).

Looking at Fig. 1 it can be seen that at any point (for example P_i inside the reacting space) radiation may be arriving from two opposite sides, since:

(i) From the outside we have a primary beam (P.B.), having a direction opposite to that of the radial coordinate ($\underline{\Omega} = -\vec{r}$). Eq. (9) with the appropriate sign can be integrated, for example, from $r = r'_2$ (where $G_\lambda = G^i_{\lambda,2}$) to $r = r$ to give:

$$G_\lambda(r)]_{P.B.} = \frac{r'_2}{r} G^i_{\lambda,2} \exp -[\beta_\lambda^{Ti(j)}(r'_2 - r)] \quad (10)$$

(ii) Outwards, we may have a secondary beam (S.B.), in which case $\underline{\Omega} = \vec{r}$ so that, after integration from $r = r^e_1$ (where $G_\lambda = G^e_{\lambda,1}$) to $r = r$, Eq. (9) gives:

$$G_\lambda(r)]_{S.B.} = \frac{r'_1}{r} G^e_{\lambda,1} \exp -[\beta_\lambda^{Ti(j)}(r - r^e_1)] \quad (11)$$

and at $r = P_i$ we will have:

$$G_\lambda(r)]_{Tot.} = G_\lambda(r)]_{P.B.} + G_\lambda(r)]_{S.B.} \quad (12)$$

Similarly, Eq. (9) can be applied to each of the annular spaces described in Fig. 1 (including the reactor walls made of Pyrex glass) to give the results shown in Tables 1 and 2.

It is apparent then that, to evaluate the Incident Radiation at any point inside the reactor when the geometry (values of

Table 1
Simplified notation

Section	Made of	Distance along r	Notation	Optical parameter	Attenuation	Notation
Outer wall	Pyrex glass	$r^e_3 - r'_3$	θ_3	κ^P_λ	$\exp-(\kappa^P_\lambda\theta_3)$	$A^P_{\lambda,3}$
III	Water	$r'_3 - r^e_2$	Δ_3	κ^R_λ	$\exp-(\kappa^R_\lambda\Delta_3)$	$A^R_{\lambda,3}$
Intermediate wall	Pyrex glass	$r^e_2 - r'_2$	θ_2	κ^P_λ	$\exp-(\kappa^P_\lambda\theta_2)$	$A^P_{\lambda,2}$
II	Actinometer 2	$r'_2 - r^e_1$	Δ_2	κ^{A2}_λ	$\exp-(\kappa^{A2}_\lambda\Delta_2)$	$A^{A2}_{\lambda,2}$
II	TiO_2 suspension	$r'_2 - r^e_1$	Δ_2	$\beta^{Ti(j)}_\lambda$ (#)	$\exp-(\beta^{Ti(j)}_\lambda\Delta_2)$	$A^{Ti(j)}_{\lambda,2}$
Inner wall	Pyrex glass	$r^e_1 - r'_1$	θ_1	κ^P_λ	$\exp-(\kappa^P_\lambda\theta_1)$	$A^P_{\lambda,1}$
I	Actinometer 1	$r'_1 - 0$	Δ_1	κ^{A1}_λ	$\exp-(\kappa^{A1}_\lambda\Delta_1)$	$A^{A1}_{\lambda,1}$

(#) j: different titanium dioxide concentrations $\beta^{Ti(j)}_\lambda = \kappa^{Ti(j)}_\lambda + \sigma^{Ti(j)}_\lambda$.

Table 2
Values of the incident radiation at selected particular locations

Position	Primary beam	Secondary beam
$r = r^e_3$	$G^e_{\lambda,3} = G_{\lambda,w}$	Negligible
$r = r'_3$	$G'_{\lambda,3} = G_{\lambda,w}\frac{r^e_3}{r'_3}A^P_{\lambda,3}$	Negligible
$r = r^e_2$	$G^e_{\lambda,2} = G'_{\lambda,3}\frac{r'_3}{r'_2}A^R_{\lambda,3}$	Negligible
$r = r'_2$	$G'_{\lambda,2} = G^e_{\lambda,2}\frac{r^e_2}{r'_2}A^P_{\lambda,2}$	Negligible
$r = r^e_1$	$G^e_{\lambda,1} = G'_{\lambda,2}\frac{r'_2}{r^e_1}A^{A2}_{\lambda,2}$	$G^e_{\lambda,1} = G'_{\lambda,1}\frac{r'_1}{r^e_1}A^P_{\lambda,3}$
$r = r^e_1$	$G^e_{\lambda,1} = G'_{\lambda,2}\frac{r'_2}{r^e_1}A^{Ti(j)}_{\lambda,2}$	
$r = r'_1$	$G'_{\lambda,1} = G^e_{\lambda,1}\frac{r^e_1}{r'_1}A^P_{\lambda,3}$	$G'_{\lambda,1} = \frac{(rG_\lambda)_{r\to 0}}{r'_1}A^{A1}_{\lambda,3}$
$r = 0$	Not required	$(rG_\lambda)_{r\to 0} = G'_{\lambda,1}r'_1A^{A2}_{\lambda,3}$

θ_1, θ_2, θ_3, Δ_1, Δ_2 and Δ_3) and the optical properties (κ_λ^P, κ_λ^R, κ_λ^{A1}, κ_λ^{A2} and $\beta_\lambda^{Ti(J)}$) of the system are known, we are left with just one unknown: the outer boundary condition $G_{\lambda,w}$ at $r = r_3^e$.

The value of the boundary condition can be obtained using emission or incidence models [19,29]. Incidence models assume that the boundary condition ($G_{\lambda,w}$ in our case) is known from an independent determination; this means that for each specific apparatus, some form of an experimental information will be required. Obviously, for reactor design purposes (particularly scale-up) incidence models are useless. Conversely, emission models can be applied to predict the boundary condition and they are very suitable for reactor design [21]. Nevertheless, for reaction kinetic studies using laboratory or bench scale units, incidence models combined with experiments can be a convenient substitute for complex lamp emission models [20,25].

Combining the equations depicted in Tables 1 and 2, it comes almost straightforwardly that the following equation applies at any point inside the reacting space II when a photocatalytic suspension circulates (see Appendix AI):

$$[G_\lambda(r)]_{Tot.}^{Ti(J)} = \frac{r_3^e}{r} G_{\lambda,w} A_{\lambda,3}^P A_{\lambda,3}^R A_{\lambda,2}^P \{\exp - [\beta_\lambda^{Ti(J)}(r_2^i - r)] + (A_{\lambda,1}^P)^2 (A_{\lambda,1}^{A1})^2 A_{\lambda,2}^{Ti(J)} \times \exp - [\beta_\lambda^{Ti(J)}(r - r_1^e)]\} \quad (13)$$

A similar equation can be developed when the actinometric solution (A2) circulates through space II; κ_λ^{A2} must be used instead of $\beta_\lambda^{Ti(J)}$ and A_2^{A2} instead of $A_2^{Ti(J)}$.

The final expression for the cylindrical space I, when the actinometric solution (A1) circulates through it is:

$$[G_\lambda(r)]_{Tot.}^{A1} = \frac{r_3^e}{r} G_{\lambda,w} A_{\lambda,3}^P A_{\lambda,3}^R A_{\lambda,2}^P A_{\lambda,2}^{Ti(J)} A_{\lambda,1}^P \times \{\exp - [\kappa_\lambda^{A1}(r_1^i - r)] + \exp - [\kappa_\lambda^{A1}(r_1^i + r)]\} \quad (14)$$

4.2. Mass balance equations (Fig. 3)

According to the expected conversion (fast or slow reaction rates), section II can be used as a once-through continuous reactor (the case of the actinometric solution A2) or as a continuous reactor inside the loop of a batch recirculating system (for the case of titanium oxide suspensions in the photocatalytic reaction). Section I will be always used as part of the loop of a batch system (owing to the very low levels of the incident radiation).

Clearly, since the activation reaction is a function of wavelengths, the oxalic acid decomposition rate $\Omega_{Ox.}(r,z)$ is a function of λ and consequently the mass balance must be derived and written for monochromatic radiation. Similar considerations apply to the photocatalytic decomposition of chloroform. Since polychromatic radiation is used, in all cases, an integration over the whole useful employed wavelengths will have to be finally performed.

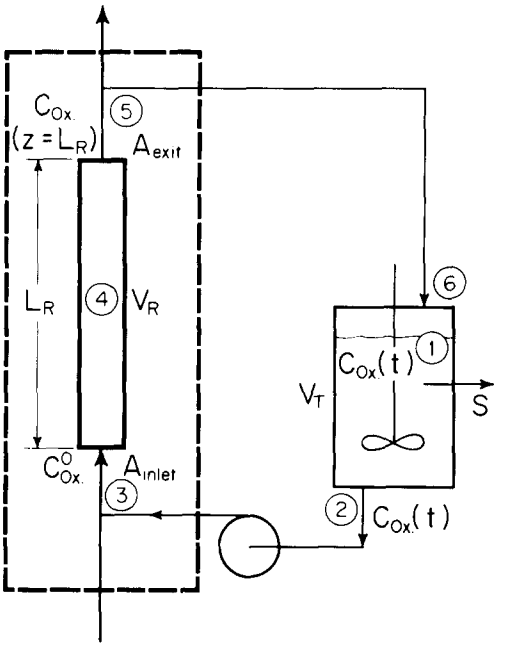

Fig. 3. Reactor mass balance. (1) Tank (batch recirculating system), (2) tank exit, (3) tubular reactor inlet, (4) continuous tubular reactor, (5) tubular reactor exit, (6) tank entrance. V_R, reactor volume; V_T, tank volume; S, sample; $C_{Ox.}$, actinometer concentration.

Case 1: Once-through reactor with the actinometric solution A1

As it is shown in Appendix AII, the following equation provides the changes in oxalic acid concentration:

$$\frac{\langle v_z \rangle}{L_R} [C_{Ox.}^0 - \langle C_{Ox.} \rangle_{A_{exit}^{II}}] = \Phi_\lambda^{Ox.} \langle e_\lambda^a(r,z) \rangle_{V_R^{II}} \quad (15)$$

Notice that the left hand side of Eq. (15) is a function of λ.

When the conversion in the actinometric reaction is kept below 20% the reaction rate follows Eq. (AII-5) and is totally independent of the oxalic acid concentration [34,35]; at the same time, for this photosensitized reaction, the uranyl concentration is independent of z. This means that $e_\lambda^a = e_\lambda^a(r)$ only, and the averaging procedure can be greatly simplified. Eq. (15) indicates that the exit concentration will be a linear function of the reactor mean residence time, and that the slope will be proportional to the VREA. Recalling Eqs. (4)–(6) and the equivalent (for the actinometer) of Eq. (13) it is clear that from these experiments the value of $G_{\lambda,w}$ can be immediately obtained (details are shown further ahead).

Case 2: Continuous reactor inside the loop of a batch recirculating system

Subcase 2.1.: Actinometric reaction in the cylindrical space I

In Appendix AIII it is shown that for the actinometer reaction in the batch recirculating system, the time evolution of the oxalic acid concentration is given by:

$$C_{Ox.}(t) = C^{0}_{Ox.} - \frac{V^{I}_{R}}{V^{I}_{T}} \Phi^{Ox.}_{\lambda} \langle e^{a}_{\lambda}(r) \rangle_{V^{I}_{R}} (t - t_0) \quad (16)$$

Recall that $C_{Ox}(t)$ is a function of λ.

Now, if $G_{\lambda,w}$ is known, using Eq. (14) and recalling Eqs. (4)–(6), one can clearly see that, when the annular space II is used as an heterogeneous photocatalytic reactor, predictions of $G(r)]^{A1}_{Tot.}$ at $r = r'_1$ (from the values of $G(r)]^{Ti(j)}_{Tot.}$ at $r = r^{e}_{2}$ using Eq. (13)) can be verified with experiments, by simply applying Eq. (16) in the cylindrical space I.

Subcase 2.2.: The photocatalytic reaction in the annular space II

If the recirculation flowrate is high the equivalent of Eq. (AIII-14) written for the organic contaminant, here represented by chloroform, takes the form:

$$\frac{dC^{Ti(j)}_{Chl.}(t)}{dt} = \frac{V^{II}_{R}}{V^{II}_{T}} \langle \Omega^{Ti(j)}_{Chl.}(r) \rangle_{V^{II}_{R}} \quad (17)$$

Once more, it must be observed that the whole Eq. (17) is a function of λ.

5. Experimental work

5.1. General description of the experimental set-up

Fig. 2 shows a schematic flow sheet of the experimental apparatus. All parts in contact with reactants were made of glass or Teflon with only one exception, as described below. The main features and dimensions are shown in Table 3. As said before, both the lamp and the reactor are located at the focal axis of a cylindrical reflector of elliptical cross section. The reactor itself is made of three precision bore, Pyrex glass concentric tubes. Since the reactor tubes (annular space II and cylindrical space I) must be cleaned very often and positioning at the focal axis of the ellipse is very critical, a special device was constructed for mounting the three concentric tubes. The radiation source was a 1200 W, high pressure, mercury arc tubular lamp, provided by Hanovia. Its operation was continuously monitored (intensity, voltage and input power), and previsions were taken to ensure the proper operation of the lamp according to its nominal input power. In accordance with the manufacturer's specifications the lamp was always used after a minimum of 100 h of operation, to make sure that it was used during the most stable period of its average life time. The reflector was made with two elliptical plates (1.25 cm thick) and a reflecting surface made of an aluminum sheet, specularly finished and furnished with Alzac treatment; it was constructed with less than 0.05 cm tolerance. Apart from the irradiated part of the reactor, all other parts of the system were blackened, to avoid any possible effect produced by laboratory or astray light. Circulation of the different reactants (actinometric solutions or titanium dioxide suspensions with substrate) was made by means of peristaltic pumps; these were the only parts of the reacting system where the fluids were in contact with Viton tubing. Other components of the apparatus are indicated in the figure captions.

It should be remarked that, permanently, two reactors were operated simultaneously: the inner cylinder (reacting space I), which always acts as an actinometric system, and the intermediate annulus (reacting space II). This second reactor can be alternatively used with the actinometric solution or with the photocatalytic system, as already stated.

Calibrated screens of different light transmission were used to change the value of the incident radiation at the outer

Table 3
Lamp, reactor and reflector characteristics

	Parameter	Value	
Lamp	Nominal power	1200	W
Hanovia LL 189A-10	Diameter	1.90	cm
High pressure	Arc length	30.48	cm
Hg vapor	Emission range	222–1367	nm
[36]	Output power	572.9	W
Reactor	Length	30	cm
Concentric	Irradiated volume *	15.75	cm^3
cylindrical	r'_1	0.16	cm
tubes made of	r'_1	0.27	cm
Pyrex glass	r'_2	0.49	cm
	r^{e}_{2}	0.61	cm
	r'_3	0.89	cm
	r^{e}_{3}	1.02	cm
Reflector	Shape	Elliptical cylinder	
Made of specularly	Length	59	cm
finished aluminium	Distance between		
with Alzac treatment	ellipse foci	43	cm
	Ellipse eccentricity	0.4	

* Reacting space II.

boundary of the reactor. These screens were made of cylindrical tubes that could be precisely positioned surrounding the reactor external tube. Exact values of the light transmission were obtained and compared by means of three separate procedures: (i) geometrical computations; (ii) spectrophotometric measurements and (iii) actinometric measurements.

5.2. Experimental procedures

Prior to initiating any experimental run a constant temperature refrigerating fluid and infrared filter, ultra pure water, was put to circulate through the annular space III; steady-state temperature could be achieved after two to three h of lamp operation. This part of the system was used to maintain the reactor (annular space II) temperature at 25 °C (it should be recalled that the Hanovia lamp has significant emission in the visible and infrared regions of the spectrum).

A concentrated actinometric solution (A1) made of a mixture of reagent grade (RG) oxalic acid (0.05 M) and RG uranyl sulfate (0.01 M) in ultra pure water recirculated through the inner tube (cylindrical space I). The reservoir (V_T^I) contained 700 ml of this solution, as well as provisions for sampling and temperature control. The device was used to measure the transmitted radiation through annular space II (i.e., the wall at $r = r_1^i$). Samples were taken at regular intervals and analyzed by conventional techniques (oxalic acid concentration by permanganimetric methods).

Through the intermediate tube (annular space II) were circulated, alternatively:

(i) A dilute actinometer aqueous solution (A2), made of a mixture of 0.025 M oxalic acid and 0.005 M uranyl sulfate, which was used to obtain the boundary condition for the Incidence model at $r = r_3^e$; i.e., $G_{\lambda,w}$. In this case the annular space was used as a once-through reactor. Sampling was made at the reactor outlet where, at the same time, the operating flow rate at steady state conditions could be measured (volumetric output during a given time interval). Flow rate stability was ensured and controlled by means of a ball flow meter and needle valve. A 50 l tank was employed to feed the reactant; the solution was continuously stirred. Analysis of the samples was made as indicated above.

(ii) The catalytic titanium dioxide suspensions [Ti(*j*)], in a recirculating loop reactor. Three different concentrations (100, 150 and 200 10^{-6} g cm^{-3}) of titanium dioxide (Aldrich; Anatase, Cat. #23,203-3) were used. The suspensions were prepared from ultra pure water and the final pH (initial for the reaction) was 6.4. The solid was previously dried at 120 °C for 12 h; then, a suspension with the desired concentration was prepared, sonicating during 60 min, and was left for stabilization during 48 h. In a separate experiment the optical stability of each of these suspensions was verified at regular intervals, during at least five days, by means of spectrophotometric determinations of the transmitted light (for more details see Ref. [37]). Prior to its use in the reactor a gentle mechanical agitation must be applied. The suspension was charged in the reactor (V_R^{II}) and the corresponding tank ($V_T^{II} = 375$ ml), and maintained under permanent stirring and circulation. Afterwards, without interruption of the vigorous agitation, oxygen (or mixtures of oxygen and nitrogen, according to the desired concentration of dissolved oxidant) was bubbled during 60 min to ensure saturation at initial conditions. The required amount of the model substrate was then added to the system, from a saturated solution of chloroform in water kept at constant temperature. The reacting system was carefully sealed, making sure that just a single fluid phase (the liquid suspension) was left. Samples were taken every 10 min and analyzed by gas chromatography with the head-space technique, using an ECD detector (Porapak Q-S, 1.80 m; 180 °C; carrier gas: nitrogen). The reactor, the recirculating reservoir and all the sampling devices were maintained at 25 °C.

6. Results

6.1. Determination of the boundary condition $G_{\lambda,w}$

Table 4 shows the wavelength dependent properties required to apply the method equations using the actinometer

Table 4
Wavelength dependent properties

Wavelength (nm)	Lamp output P_λ (Einstein $s^{-1} \times 10^6$) [36]	Pyrex glass κ_λ^P (cm^{-1})	Actinometer α_λ^A (cm^2 $gmol^{-1} \times 10^{-3}$) [38–40]	Actinometer Φ_λ (g mol Einstein^{-1}) [38–40]
280	32.50	65.00	3445	0.58
289	10.60	54.11	2476	0.58
296	37.60	40.00	1880	0.57
302	83.00	16.63	1489	0.56
313	132.00	10.96	1023	0.56
334	19.30	4.95	366	0.52
366	297.00	2.12	40.9	0.49
404	81.70	1.60	36.5	0.56
435	193.00	1.41	32.5	0.58
546	185.00	1.41	0.25	0.02
578	335.00	1.23	0.25	0.02

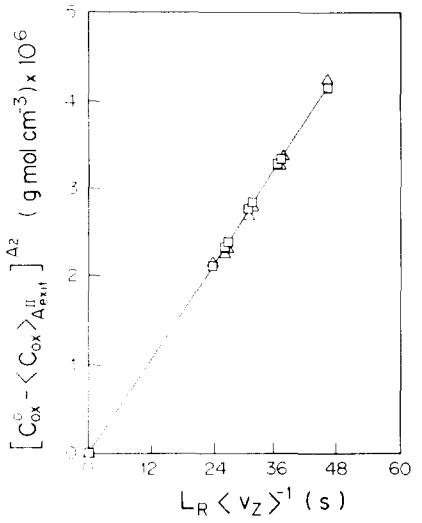

Fig. 4. Actinometer experimental results 1. Verification of the theoretical predictions of Eq. (15) (needed to determine $G_{\lambda,w}$, with Eq. (23)). Space II: oxalic acid-uranyl oxalate actinometric solution. Oxalic acid decomposition $[C^0_{Ox} - \langle C_{Ox}\rangle_{A^{II}_{exit}}]^{A2}$ vs. $L_R/\langle v_z\rangle$ (mean residence time). △, experimental values; □, linear regression values.

in the annular space II. Fig. 4 presents experimental results obtained from a set of runs made with no radiation screens in the system. The linear dependence of the exit concentration ($z = L_R$) with the average retention time in the reactor ($L_R/\langle v_z\rangle$) is clearly established, according to Eq. (15).

The experimental results are evaluated as follows: in the R.H.S. of Eq. (15) let us substitute e^a_λ according to Eqs. (4) and (6); then, one can replace the value of G_λ using the actinometer version of Eq. (13). The result is:

$$\Phi^{Ox}_\lambda \langle e^a_\lambda \rangle_{V^{II}_R} = \Phi^{Ox}_\lambda G_{\lambda,w} r^e_3 \kappa^{A2}_\lambda A^P_{\lambda,3} A^R_{\lambda,3} A^P_{\lambda,2} \times \left\langle \frac{1}{r} \{ [\exp - \kappa^{A2}_\lambda (r^i_2 - r)] + (A^P_{\lambda,1})^2 (A^{A1}_{\lambda,1})^2 A^{A2}_{\lambda,2} \times [\exp - \kappa^{A2}_\lambda (r - r^e_1)] \} \right\rangle_{V^{II}_R} \quad (18)$$

Solving for the volume average indicated in Eq. (18) and applying Eq. (15):

$$\frac{2 r^e_3 G_{\lambda,w} \Phi^{Ox}_\lambda}{[(r^i_2)^2 - (r^e_1)^2]} A^P_{\lambda,3} A^R_{\lambda,3} A^P_{\lambda,2} [\{1 - \exp[-\kappa^{A2}_\lambda (r^i_2 - r^e_1)]\} + (A^P_{\lambda,1})^2 (A^{A1}_{\lambda,1})^2 A^{A2}_{\lambda,2} \{1 - \exp[-\kappa^{A2}_\lambda (r^i_2 - r^e_1)]\}] = \frac{\langle v_z \rangle}{L_R} [C^0_{Ox} - \langle C_{Ox}\rangle_{A_{exit}}]_\lambda \quad (19)$$

At low concentrations Beer's approximation applies:

$$\kappa^{A2}_\lambda = \alpha^A_\lambda C^{A2}_{Ur.\ Ox} \quad (20)$$

One can assume that at $r = r^e_3$ the spectral distribution of the lamp output power is maintained (the response of the reflector in the wavelength range under consideration is flat):

$$G_{\lambda,w} = \frac{G_{tot,w} P_\lambda}{P_{tot}} \quad (21)$$

Strictly speaking this assumption is somehow critical below 310 nm. According to Koller [41] the aluminum reflector with Alzak treatment (the one used in this work) has a spectral reflectance that varies from 75% to 83% when one moves from 310 nm to over 450 nm. This small variation in the spectral reflectance has been confirmed in our laboratory using the model 1413 Specular Reflectance Accessory of our Cary 17 DHC U.V.-Visible Spectrophotometer, even though in our case we have consistently observed lower values (always a small variation from 310 to 500 nm, but always with a reflectance below 80%). Form 280 to 310 nm the spectral variation of the reflection coefficient is more important. In our work (see Table 5) this effect could have some influence mainly in the results corresponding to the 302 nm line of emission of the lamp and below. The emission from 280 to 310 nm represents approximately 11.6% of the total radiation arriving at the reactor boundaries and, consequently, the error introduced will not alter significantly the final results. This statement is valid for a reflecting surface used with great care, in a clean environment and, as a matter of precaution, for an experimental work performed within a 30 month period from the moment in which the packing plastic protecting cover of the reflector was removed from it.

It is worth noticing that the equations used (starting from Eq. (21) on) can be easily corrected by introducing a normalized, wavelength dependent reflection coefficient for each of the significant emission lines of the lamp.

Under these conditions, following the procedures described in detail by Clariá et al. [42] one can apply Eq. (3) and extend Eq. (19) to polychromatic radiation. Now defining

$$\Theta_\lambda = \{1 - \exp[-\kappa^{A2}_\lambda (r'_2 - r^e_1)]\} + (A^P_{\lambda,1})^2 (A^{A1}_{\lambda,1})^2 A^{A2}_{\lambda,2} \{1 - \exp[-\kappa^{A2}_\lambda (r'_2 - r^e_1)]\} \quad (22)$$

and solving for the boundary condition one finally obtains:

Table 5
Spectral incident radiation values (boundary condition)

Wavelength (λ) (nm)	$G_{\lambda,w}$ (Einstein cm^{-2} s^{-1} × 10^8)
280	1.68
289	0.53
296	1.95
302	4.30
313	6.83
334	0.98
366	15.36
404	4.23
435	9.98
546	9.56
578	17.33
$G_{tot,w}$ =	72.73

Table 6
Screen transmission values

Screen	Transmission (%)		
	Calculated (geometry)	Spectrophotometer	Actinometer
0 *	100	100	100
I	66	–	65.6
II	40	≈39	39.5
III	29	≈28	27.5
IV	6	–	5.7

* No screen.

$$G_{\lambda,w}=\frac{P_\lambda Q[(r_2^i)^2-(r_1^e)^2]\left\{\sum_{\lambda=280\text{ nm}}^{\lambda=578\text{ nm}}[C_{Ox.}^0-\langle C_{Ox.}\rangle_{A_{exit}}]_\lambda\right\}}{2V_R^{II}r_3^e\left\{\sum_{\lambda=280\text{ nm}}^{\lambda=578\text{ nm}}P_\lambda[A_{\lambda,3}^P A_{\lambda,3}^R A_{\lambda,2}^P \Phi_\lambda^{Ox.}\{\Theta_\lambda\}]\right\}} \quad (23)$$

In Eq. (23) both concentration of oxalic acid, the volumetric flow rate and the reactor volume are known from experiments; also, the upper and lower wavelength limits in the summation symbol correspond to the maximum spectral line of the lamp where the absorbance of the uranyl ion is still measurable and the Pyrex cutoff wavelength, respectively. The geometric dimensions (r_k^i) are known and the absorption coefficients (κ_k^q) can be measured with a spectrophotometer. Then, the attenuation (A_k^q) can be calculated using the definitions given in Table 1 and the values from Table 4. Quantum yields are known from the literature and P_λ values can be obtained from the lamp manufacturer specifications (Table 4). Consequently, $G_{\lambda,w}$ can be known. The results for our experimental set-up are indicated in Table 5.

As it was described before, other values of the boundary condition were obtained, by using different cylindrical screens surrounding the reactor. The percent transmission of the different combinations employed, according to the three methods of measurement previously described are indicated in Table 6, showing an excellent agreement among them. Incidentally, the spectrophotometric measurements showed that the screens percent transmission values were uniform across the full wavelength range, as expected.

6.2. Verification of the FIP operation

The FIP operation can be confirmed if a measurable reaction can be obtained in the cylindrical space I while a given titanium dioxide suspension circulates through the annular reacting space II. Additionally, if this verification is made with enough accuracy the experimental results, obtained in this case with the concentrated actinometer solution (A1), can be used to get a quantitative evaluation of the goodness of the single scattering approximation. Under the experimental conditions already stated, the decomposition of the uranyl oxalate complex into the reacting space I can be accurately measured, by simply recirculating the solution inside the loop of the batch system. Then, if the approximation to Eq. (1) given by Eq. (7) applies, its use to predict the outgoing radiation from $r=r_1^e$ can be tested. So, correcting to account for the absorption due to the Pyrex glass wall (Δ_1), the value of G_λ at $r=r_1^i$ can be obtained.

In mathematical terms, if the approximation is reasonably good, the incoming radiation into reacting space I should be given by:

$$\sum_{\lambda=280\text{ nm}}^{\lambda=578\text{ nm}}[G_\lambda(r=r_1^i)]_{Tot.}$$
$$=\frac{r_3^e}{r_1^i}\sum_{\lambda=280\text{ nm}}^{\lambda=578\text{ nm}}G_{\lambda,w}A_{\lambda,3}^P A_{\lambda,3}^R A_{\lambda,2}^P A_{\lambda,2}^{Ti(IV)} A_{\lambda,1}^P$$
$$\times[1+\exp-(2\kappa_\lambda^{A1}r_1^i)] \quad (24)$$

The absorption coefficient for the actinometer in this case, from the Beer's approximation, is

$$\kappa_\lambda^{A1}=\alpha_\lambda^A C_{Ur.-Ox.}^{A1} \quad (25)$$

Then, applying Eqs. (4–6), (14), (AII-5), (24) and (25) to the cylindrical reactor with polychromatic radiation, the predicted reaction rate should be:

$$\left\{\sum_{\lambda=280\text{ nm}}^{\lambda=578\text{ nm}}\langle\Omega_\lambda^{Ox.}\rangle_{V_R^I}\right\}_{A1}$$
$$=-\left(\frac{2}{r_1^i}\right)\sum_{\lambda=280\text{ nm}}^{\lambda=578\text{ nm}}\Phi_\lambda^{Ox.}\{[G_\lambda(r=r_1^i)]_{Tot.}$$
$$\times[1-\exp(-2\kappa_{\lambda,1}^{A1}r_1^i)]\} \quad (26)$$

These results must be compared with the experimental reaction rate than can be obtained by integration of Eq. (AIII-14):

$$\left\{\sum_{\lambda=280\text{ nm}}^{\lambda=578\text{ nm}}\langle\Omega_\lambda^{Ox.}\rangle_{V_R^I}\right\}_{A1}=\frac{V_T^I}{V_R^I}\frac{[C_{Ox.}(t=t)-C_{Ox.}(t=t_0)]}{t-t_0} \quad (27)$$

The expected linearity of the reactant conversion versus reaction time (Eq. (16)) is shown in Fig. 5; also, dilute suspensions of this type of commercial titanium dioxide allow the use of a specific extinction coefficient to characterize them [43], as it is explained below in full detail. Results of the comparison indicated by Eqs. (26) and (27) are shown in Table 7. One can conclude that for this particular experimental set-up and the employed catalyst concentrations the radial model and the single scattering approximations can be used with confidence.

6.3. Quantum efficiencies

Quantum efficiencies (for polychromatic radiation) were obtained for the photocatalytic decomposition of chloroform.

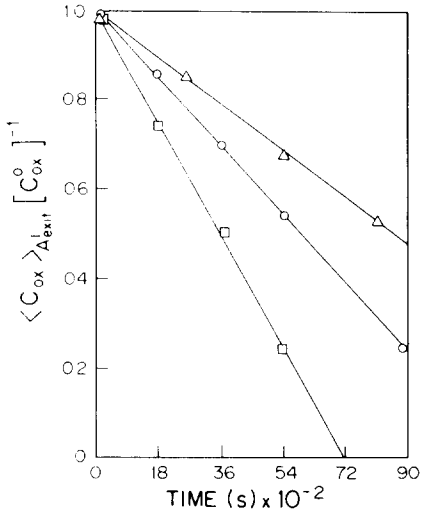

Fig. 5. Actinometer experimental results 2. Verification of the theoretical predictions of Eq. (16). Space II: suspended titania, △ 200, ○ 150, □ 100 (g cm^{-3}) × 10^6. Space I: oxalic acid-uranyl oxalate actinometric solution. Dimensionless oxalic acid concentration (C_{ox}/C_{ox}^0) vs. reaction time (s).

Table 7
Reaction rates for actinometries in space I

Catalyst concentration (g cm^{-3} × 10^6)	Predictions Eq. (26) (gmol cm^{-3} s^{-1} × 10^8)	Experiments Eq. (27) (gmol cm^{-3} s^{-1} × 10^8)
200	14.45	15.50
150	22.50	19.80
100	34.33	35.56

The employed catalyst loadings were: 100, 150 and 200×10^{-6} g cm^{-3}. The initial concentration of the substrate was changed from 10 to 100×10^{-9} gmol cm^{-3} (10–100 μM). Incident Radiation at $r = r_3^e(G_{\lambda,w})$ was varied from the full values indicated in Table 5 (i.e. without screen), down to about 6% of them, when the smallest screen was placed. The initial concentration of oxygen ranged from 21% (air) to 100% (pure gas); a total of three different levels was used.

For the reactant disappearance, the pseudo-homogeneous system quantum yield (employing monochromatic radiation) has been usually defined as follows [24,44]:

$$\Phi_\lambda^{\text{Re act.}} = \frac{(\text{No. of moles decomposed})_\lambda}{(\text{No. of einstein absorbed})_\lambda} = \frac{(-\text{Reactant Reaction Rate})_\lambda}{(\text{Radiation Absorption Rate})_\lambda} = \frac{[\langle -\Omega_\lambda^{\text{Re act.}}(r)\rangle_{V_R^{II}}]_{Ti(f)}}{[\langle e_\lambda^a(r)\rangle_{V_R^{II}}]_{Ti(f)}} \quad (28)$$

We have already noticed, for our particular case, the radial dependence of both rates. For polychromatic radiation a pseudo-homogeneous system quantum efficiency can be used [24,45]:

$$\eta_{\Sigma\lambda}^{\text{Re act.}} = \frac{\left[\sum_\lambda -\langle \Omega_\lambda^{\text{Re act.}}(r)\rangle_{V_R^{II}}\right]_{Ti(f)}}{\left[\sum_\lambda \langle e_\lambda^a(r)\rangle_{V_R^{II}}\right]_{Ti(f)}} \quad (29)$$

The reaction rate must be specified at given conditions of concentration, temperature, pH, catalyst loading, etc., and measured at a given reaction time, for example, at initial conditions.

The numerator of Eq. (29) is an experimental value that can be calculated according to Eq. (17), from:

$$\left[\sum_\lambda -\langle \Omega_\lambda^{\text{Re act.}}(r)\rangle_{V_R^{II}}\right]_{Ti(f)} = \frac{V_T^{II}}{V_R^{II}} \lim_{t\to 0} \left\{\frac{C_{Chl.}|_{t\ \ t} - C_{Chl}|_{t\ \ t_0}}{t - t_0}\right\} \quad (30)$$

On the contrary, from Eqs. (4–6) and (13), the denominator of Eq. (29) is:

$$\left[\sum_\lambda \langle e_\lambda^a(r)\rangle_{V_R^{II}}\right]_{Ti(f)} = \frac{2r_3^e}{[(r_2')^2 - (r_1^e)^2]} \sum_{\lambda=280\text{ nm}}^{\lambda=380\text{ nm}} \left\{G_{\lambda,w} A_{\lambda,3}^P A_{\lambda,3}^R A_{\lambda,2}^P \frac{\kappa_\lambda^{Ti,*}}{\beta_\lambda^{Ti,*}}\right\} \times \{\{1 - \exp[-\beta_\lambda^{Ti(f)}(r_2' - r_1^e)]\} + (A_{\lambda,1}^P)^2 (A_{\lambda,1}^{AI})^2 A_{\lambda,2}^{Ti(f)} \{1 - \exp[-\beta_\lambda^{Ti(f)}(r_2' - r_1^e)]\}\} \quad (31)$$

In this case, the limits of the wavelengths employed in Eq. (31) are set as follows: the lamp has emission lines from $\lambda = 200$ nm to $\lambda = 1367$ nm; however: (i) the radiation must cross two Pyrex walls before reaching reacting space II and hence $\lambda_{min} \cong 280$ nm, and (ii) the photoactive (i.e., photocatalytic) interaction of semiconductive materials with light is defined by the size of their bandgap, so that in the case of titanium dioxide particles any relevant absorption begins below 380 nm; thus, $\lambda_{max} \cong 380$ nm.

In Eq. (31) we have used κ_λ and β_λ written as the product of specific (per unit mass) absorption and extinction coefficients times the photocatalyst mass concentration, both defined as follows:

$$\kappa_\lambda^{Ti(f)} = \kappa_\lambda^{Ti,*} C_m^{Ti(f)} \quad (32)$$

$$\beta_\lambda^{Ti(f)} = \beta_\lambda^{Ti,*} C_m^{Ti(f)} \quad (33)$$

Considering the information required for Eq. (31) and that used in Eqs. (22) and (23) we must add now the values of the specific absorption and extinction (absorption plus scattering) coefficients to be used in Eqs. (32) and (33).

Spectrophotometric measurements with the suspension of the heterogeneous sample produce a value that can be at its best, when scattering-in is minimized, an extinction coefficient. Indeed, in the 0–200 ppm range, using conventional

Table 8
Optical properties of the titanium oxide suspensions (Aldrich Cat. No. 23,023-3)

Wavelength (λ) (nm)	$\beta_\lambda^{Ti,*}$ ($cm^2\ g^{-1} \times 10^{-3}$) [37]	$\kappa_\lambda^{Ti,*}$ ($cm^2\ g^{-1} \times 10^{-3}$) [24]
280	32.78	4.17
289	32.96	4.19
296	33.10	4.20
302	33.30	4.22
313	33.49	4.54
334	34.52	4.52
366	37.18	1.46
404	40.12	0.00
435	41.98	0.00

Mass specific properties of the suspensions are valid for the employed experimental preparation protocol and concentration range used in this work.

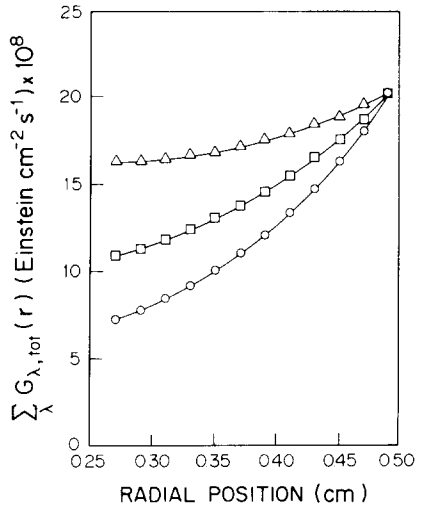

Fig. 6. Total incident radiation distribution inside the photoreactor vs. radial position (Eq. (13)). Space II: suspended titania concentration used in the experimental program, △ 100, □ 150, ○ 200 (g cm^{-3}) × $10^6 \cdot r_1^e = 0.27$ cm; $r_2^i = 0.49$ cm (unscreened reactor).

cuvettes of 0.5 cm path length, specific extinction coefficients of the Aldrich type titanium dioxide could be readily obtained by one of us [37]. However, a different, independent measurement is required to obtain absorption coefficients. To obtain the absorption coefficient Cabrera et al. [24,25] have used a combination of conventional spectrophotometric measurements and special experiments placing an integrating sphere at the outlet of the spectrophotometer sample cell. This last type of detection collects all the non-absorbed photons that are scattered in the forward direction. As said before, almost conventional measurements can give the specific extinction coefficient (if and when provisions are taken to minimize the scattering-in and maximize the scattering-out). However, with a good degree of approximation, the results of the measurements with the integrating sphere provided a value that can be associated with that energy corresponding to forward scattering. The most simple radiative transfer model was applied to the spectrophotometer cell; thus, for each wavelength, the energy measured by the integrating sphere detector could be predicted using just a single adjustable parameter: the specific absorption coefficient (because the specific extinction coefficient was known from independent determinations). Using a non-linear least square fitting, handled by an optimization program, this adjustment was made employing the model output and the experimental results. Table 8 provides the specific values (i.e., per unit particle mass concentration) of the extinction and absorption coefficients, as a function of wavelength, for the titanium oxide suspension used in this work [24,37].

Fig. 6 shows a representation of Eq. (13) from $r = r_2^i$ to $r = r_1^e$ and polychromatic radiation, i.e.:

$$\sum_{\lambda=280\ nm}^{\lambda=380\ nm} G_{\lambda,tot}(r) \text{ vs. } r \qquad (34)$$

for the three catalyst concentrations employed in this work. Clearly, radiation attenuation is greatly increased with an increase in the catalyst concentration. Similarly, Fig. 7 shows for the same region results corresponding to the polychromatic LVREA, i.e.:

$$\sum_{\lambda=280\ nm}^{\lambda=380\ nm} e_\lambda^a(r) \text{ vs. } r \qquad (35)$$

This representation shows the way by which the incident radiation radial profiles depicted in Fig. 6 are modified by the local absorption. From these last results one should be expecting a significant difference between reaction rates at positions close to $r = r_2^i$ and those close to $r = r_1^e$, particularly when $C_m^{Ti} = 0.200 \times 10^{-3}$ g cm^{-3}. For larger values of the catalyst loading or the distance ($r_2^i - r_1^e$) one can certainly foresee the possibility of a change in the reaction mechanism from one place to the other; for instance, if the lower values of the incident radiation become much smaller than those corresponding to one sun [46–48].

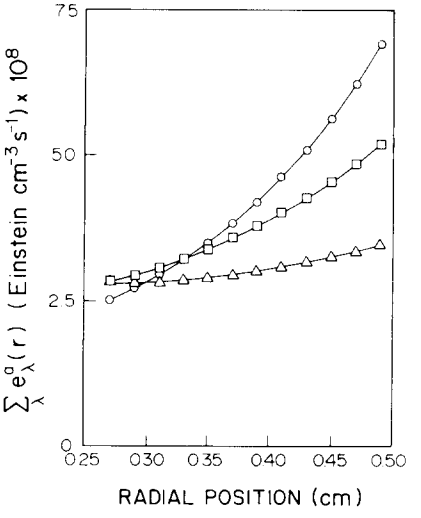

Fig. 7. Total LVREA distribution inside the photoreactor vs. radial position (Eq. (35)). Space II: suspended titania concentration used in the experimental program. △ 100, □, 150, ○ 200 (g cm^{-3}) × $10^6 \cdot r_1^e = 0.27$ cm; $r_2^i = 0.49$ cm (unscreened reactor).

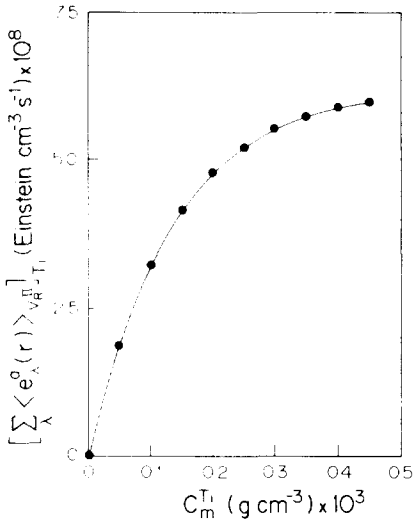

Fig. 8. Reactor volume averaged values of the total LVREA vs. catalyst concentration (obtained with Eq. (36)), (unscreened reactor).

One interesting observation can be derived by representating the reactor volume averaged radiation absorption rate versus the catalyst concentration, i.e.,

$$\left[\sum_\lambda \langle e^a_\lambda(r)\rangle_{V^{III}_R}\right] \text{ vs. } C_m^{Ti(f)} \qquad (36)$$

This information (Fig. 8) indicates that, in regards to the optimal utilization of the available radiation arriving at $r = r_2'$ for a reactor thickness of this size (0.22 cm), a catalyst concentration of 0.5 to 0.6×10^{-3} g cm^{-3} should be enough. Any increase in the catalyst concentration beyond this limit (for this reactor thickness) should not produce a sensible effect in the reaction rate as far as the radiation level effect is concerned.

Table 9 shows values of the initial reaction rate and calculated quantum efficiencies corresponding to different operating conditions of the reactor. It can be readily seen that an increase in the substrate concentration has a significant, positive effect on the quantum efficiency and also that a decrease in the average value of the absorbed radiation, owing to the use of attenuation screens that modify the value of the incident radiation at the boundary condition, leads to a sensible increase of η. It is worth noticing at this point that a decrease in the average value of the absorbed radiation can also be produced by simply changing the catalyst concentration (cf., runs 3, 7 and 10). However, it can be observed that: (i) when the catalyst concentration was decreased by a factor of 2 (runs 3 and 10) the quantum efficiency was just slightly modified, whereas (ii) when the incident radiation ($G_{tot,w}$) was decreased (by a factor of 3.5 (runs 3 and 27)) the quantum efficiency increased by a factor of almost 2.3. This last observation is of utmost importance, because it strongly suggests that better, more efficient photocatalytic devices are certainly not the ones furnished with the highest incident radiation level. Under the explored conditions no significant effect on η was observed as a consequence of changes in the oxygen concentration (runs 3, 15 and 19 for example). In a separate contribution, a more detailed and quantitative analysis of these trends is made, within the framework of the reaction kinetics proper [43].

These values of quantum efficiencies are just valid for the employed conditions, namely: catalyst type and catalyst concentrations, substrate concentrations, ranges of irradiation and/or the initial pH of the aqueous solutions. To the best of our knowledge, there is no evidence so far that these reported values can be extended to other operating conditions different from the ones indicated in this paper. However, we think that this method provides reliable results of the LVREA, and hence that, when the operating conditions are well defined, it can be used with confidence to calculate quantum efficiencies (or quantum yields, for monochromatic radiation).

7. Conclusions

Form the above reported results it can be concluded that:

(1) The proposed reactor operates as a fully irradiated photocatalytic (FIP) reactor. When it is used for kinetic

Table 9
Quantum efficiencies for the chloroform decomposition *

Run number	C^0_{Chl} (g mol cm^{-3} x 10^9)	C^0_{Oxy} (g mol cm^{-3} x 10^9)	C^{Ti}_m (g cm^{-3} x 10^6)	Transmission (%)	$\sum_\lambda \langle \Omega^{Chl}_\lambda \rangle_{V^{III}_R}$ (g mol cm^{-3} s^{-1} x 10^{11})	$\sum_\lambda \langle e^a_\lambda \rangle_{V^{III}_R}$ (Einstein cm^{-3} s^{-1} x 10^{11})	η (%)
1	90	1200	200	100	22.50	4683	0.48
2	55	1200	200	100	16.00	4683	0.34
3	29	1200	200	100	7.20	4683	0.15
7	29	1200	150	100	5.91	4066	0.15
10	30	1200	100	100	5.50	3166	0.17
15	24	720	200	100	6.00	4683	0.13
19	25	250	200	100	6.68	4683	0.14
23	27	1200	200	66	6.11	3100	0.20
27	29	1200	200	29	4.00	1191	0.34
31	38	1200	200	6	4.95	275	1.8

* Room temperature, 298 K; initial pH = 6.4.

studies it allows us to know for a certainty that all the catalyst mass that is present in the reactor receives radiation and can be photoactivated. This type of operation was experimentally verified beyond doubt.

(2) The proposed combination of simple radiation and reactor models with specially designed experiments (employing classic actinometric solutions) permits all the information required to compute the LVREA in the photocatalytic reactor to be obtained. But it should be stressed that, in this method, homogeneous actinometry is solely used to measure $\sum_\lambda G_{\lambda,w}$ at $r = r_3^e$.

(3) Under the employed experimental conditions it was also shown that the knowledge of the extinction coefficient of any given suspension of the photocatalyst $[\beta_\lambda^{Ti(j)}]$ is enough to know the radial distribution of the incident radiation $[G_\lambda(r)]$ inside the reactor; the good agreement between results of Eqs. (26) and (27) is a clear indication of it. However, the absorption coefficient $[\kappa_\lambda^{Ti(j)}]$ of the suspension must be known to compute the radial profile of the LVREA $[e_\lambda^a(r)]$. This is so, because it is known that in order to compute the absorbed energy, the use of the extinction coefficient instead of the absorption coefficient, overestimates the radiation absorption rate and underestimates the quantum efficiency [24,25].

(4) With the proposed method, quantum efficiencies (or quantum yields if monochromatic radiation sources were used) can be computed with good confidence. For the chloroform decomposition in particular, under the investigated experimental conditions, it was found that the quantum efficiency: (i) increases when the initial concentration of substrate is augmented, (ii) is almost insensitive to the initial concentration of dissolved oxygen and (iii) increases at lower levels of the volume-averaged absorbed radiation. This last result seems to be typical of photoreacting devices where the levels of incident radiation are moderate (i.e., close to one sun equivalent) [49–51].

(5) For a characteristic distance of $r_2^i - r_1^e = 0.22$ cm a catalyst concentration of about $0.5\text{–}0.6 \times 10^{-3}$ g cm^{-3} is sufficient to render an opaque reactor.

Acknowledgements

The authors are grateful to Consejo Nacional de Investigaciones Científicas y Técnicas (CONICET) and to Universidad Nacional del Litoral (U.N.L.) for their support to produce this work. They also thank Prof. Orlando M. Alfano for his participation in helpful discussions about the results presented in this paper.

Special mention is made to Deutsche Gesellschaft für Technische Zusammenarbeit (GTZ) GmbH for an Equipment Grant under Program PN 87.2061.7-02.300/9357.

Appendix AI

Incident radiation within the photocatalytic reactor space

Applying Eqs. (10) and (11) to the photocatalytic suspension one gets:

$$[rG_\lambda(r)]_{P.B.} = r_3^e G_{\lambda,w} A_{\lambda,3}^P A_{\lambda,3}^R A_{\lambda,2}^P \exp - [\beta_\lambda^{Ti(j)}(r_2^i - r)] \quad \text{(AI-1)}$$

$$[rG_\lambda(r)]_{S.B.} = r_3^e G_{\lambda,w} A_{\lambda,3}^P A_{\lambda,3}^R A_{\lambda,2}^P (A_{\lambda,1}^P)^2 (A_{\lambda,1}^{A1})^2 A_{\lambda,2}^{Ti(j)} \times \exp - [\beta_\lambda^{Ti(j)}(r - r_1^e)] \quad \text{(AI-2)}$$

In Eq. (AI-2) we have:

$$[rG_\lambda(r)]_{r\to 0} = r_3^e G_{\lambda,w} A_{\lambda,3}^P A_{\lambda,3}^R A_{\lambda,2}^P A_{\lambda,1}^P A_{\lambda,1}^{A1} A_{\lambda,2}^{Ti(j)} \quad \text{(AI-3)}$$

And lastly, with Eq. (12), one gets the final result indicated by Eq. (13).

Appendix AII

Mass balance for once-through reactor with the actinometer solution A1 (Fig. 3)

At steady state [30]:

$$\underline{\nabla} \cdot \underline{N}_{Ox.}(r,z) = \Omega_{Ox.}(r,z) \quad \text{(AII-1)}$$

with the initial condition:

$$C_{Ox.}(r,z=0) = C_{Ox.}^0 \quad \text{(AII-2)}$$

and the boundary conditions:

$$\underline{N}_{Ox.}(r = r_2^i, z) = 0 \quad \text{(AII-3)}$$

$$\underline{N}_{Ox.}(r = r_2^e, z) = 0 \quad \text{(AII-4)}$$

Under controlled conditions the uranyl oxalate decomposition reaction is of first order with respect to the LVREA and of zero order with respect to the oxalic acid concentration [31–33]. Moreover, the uranyl ion is not consumed. Then, the reaction rate for the oxalic acid decomposition is given by:

$$\Omega_{Ox.}(r,z) = -\Phi_\lambda^{Ox.} e_\lambda^a(r,z) \quad \text{(AII-5)}$$

Let us substitute Eq. (AII-5) and integrate over the reactor volume:

$$\int_{V_R^{II}} \underline{\nabla} \cdot \underline{N}_{Ox.}\, dV = \int_{A_R^{II}} (\underline{N}_{Ox.} \cdot \underline{n})\, dA = -\Phi_\lambda^{Ox.} \int_{V_R^{II}} e_\lambda^a\, dV \quad \text{(AII-6)}$$

In Eq. (AII-6) the divergence theorem has been applied. Solving the surface integral, applying the boundary conditions given by Eqs. (AII-3) and (AII-4), recalling that $\underline{N}_{Ox.} = C_{Ox.}\underline{v}_{Ox.}$ and neglecting diffusional fluxes when compared with the convective flow in the liquid phase $\underline{v}_{Ox.} \cdot \underline{e} = v_z(r)$]:

$$\int_{A^{II}_{exit}} C_{Ox.}(r,z=L_R)v_z(r)\,dA - \int_{A^{II}_{inlet}} C^0_{Ox.}v_z(r)\,dA = -\Phi^{Ox.}_\lambda \int_{V^{II}_R} e^a_\lambda(r,z)\,dV \quad \text{(AII-7)}$$

In Eq. (AII-7) the initial condition (Eq. (AII-2)) was applied. With the following conventional definitions:

$$\langle v_z\rangle = \frac{\int_A v_z(r)\,dA}{A} \quad \text{(AII-8)}$$

$$\langle C_i(r,z=L_R)\rangle = \frac{\int_A C_i(r,z=L_R)v_z(r)\,dA}{\langle v_z\rangle A} = \langle C_{Ox.}\rangle_{A_{exit}} \quad \text{(AII-9)}$$

and, recalling Eq. (6), the spectral VREA is given by:

$$\langle e^a_\lambda(r,z)\rangle_{V_R} = \frac{\int_{V_R} e^a_\lambda(r,z)\,dV}{V_R} \quad \text{(AII-10)}$$

Combining Eqs. (AII-7) to (AII-10) one obtains Eq. (14).

Appendix AIII

Mass balance for the actinometer reaction in the cylindrical space I (Fig. 3). Continuous reactor inside the loop of a batch recirculating system

The mass balance equation [30] is:

$$\frac{\partial C_{Ox.}(\underline{r},t)}{\partial t} + \underline{\nabla}\cdot\underline{N}_{Ox.}(\underline{r},t) = \Omega_{Ox.}(\underline{r},t) \quad \text{(AIII-1)}$$

Let us look at space ① in Fig. 3:

Inside the tank (V^I_T), assuming very good mixing, concentration is only a function of time [$C_{Ox.} \neq C_{Ox.}(\underline{r})$ and $C_{Ox.} = C_{Ox.}(t)$]. When the sampling volume is negligible $V^I_T \neq V^I_T(t)$; if this is not the case, corrections will be necessary but all the equations will still be valid between sampling intervals. As the tank is not illuminated, the reaction rate will be zero. Integrating Eq. (AIII-1) over the tank volume (that is, the volume occupied by the liquid phase):

$$\int_{V^I_T} \frac{\partial C_{Ox.}(t)}{\partial t}\,dV = \frac{dC_{Ox.}(t)}{dt} V^I_T = -\int_{A^I_T} (\underline{n}\cdot\underline{N}_{Ox.})\,dA \quad \text{(AIII-2)}$$

At the tank walls we have boundary conditions equivalent to those represented by Eq. (AII-3) and (AII-4); then, $\underline{N}_{Ox}$ is different from zero only at its entrance and exit surfaces. At the tank exit, ②, the oxalic concentration is $C_{Ox.}(t)$; at the tank entrance, ⑥, the oxalic concentration is the same as the exit concentration from the reactor, $\langle C_{Ox.}\rangle_{A^I_{exit}}$ at ⑤. Recalling the definition:

$$Q = \int_A v_z(r)\,dA \quad \text{(AIII-3)}$$

and since under hydrodynamic steady state $Q_{out} = Q_{in} = Q$ we have:

$$\frac{dC_{Ox.}(t)}{dt} V^I_T = |\langle C_{Ox.}(r,z=L_R,t)\rangle_{A^I_{exit}} - C_{Ox.}(t)|\,Q \quad \text{(AIII-4)}$$

Turning now our attention to space ④ in Fig. 2, Eq. (AIII-1) can be integrated over the reactor volume:

$$\int_{V^I_R} \frac{\partial C_{Ox.}(r,z,t)}{\partial t}\,dV + \int_{A^I_R} (\underline{n}\cdot\underline{N}_{Ox.})\,dA = \int_{V^I_R} \Omega(r,z,t)\,dV \quad \text{(AIII-5)}$$

The following definitions can be used:

$$\langle C_{Ox.}(r,z,t)\rangle_{V^I_R} = \frac{\int_{V^I_R} C_{Ox.}(r,z,t)\,dV}{V^I_R} \quad \text{(AIII-6)}$$

$$\langle \Omega_{Ox.}(r,z,t)\rangle_{V^I_R} = \frac{\int_{V^I_R} \Omega_{Ox.}(r,z,t)\,dV}{V^I_R} \quad \text{(AIII-7)}$$

Since $\langle C_{Ox.}(r,z,t)\rangle_{V^I_R}$ is not a function of r or z, $\langle C_{Ox.}(r,z=0,t)\rangle_{A^I_{inlet}}$ is only a function of t and $V^I_R \neq V^I_R(t)$ under hydrodynamic steady state we have:

$$V^I_R \frac{d\langle C_{Ox.}(r,z,t)\rangle_{V^I_R}}{dt} + [\langle C_{Ox.}(r,z=L_R,t)\rangle_{A^I_{exit}} - C_{Ox.}(t)]Q = \langle \Omega_{Ox.}(r,z,t)\rangle_{V^I_R} V^I_R \quad \text{(AIII-8)}$$

Adding Eq. (AIII-4) and (AIII-8), and considering that $V^I_R + V^I_T \cong V^I_{tot}$ (i.e., neglecting connecting lines volumes):

$$\frac{d}{dt}\left[\frac{V^I_T}{V^I_{tot.}} C_{Ox.}(t) + \frac{V^I_R}{V^I_{tot.}}\langle C_{Ox.}(r,z,t)\rangle_{V^I_R}\right] = \frac{d\langle C_{Ox.}(r,z,t)\rangle_{V^I_{tot}}}{dt} = \frac{V^I_R}{V^I_{tot}}\langle \Omega_{Ox.}(r,z,t)\rangle_{V^I_R} \quad \text{(AIII-9)}$$

Equation (AIII-9), as shown, is difficult to handle. However, from Eqs. (AIII-4) and (AIII-8), if

$$\frac{d\langle C_{Ox.}(r,z,t)\rangle_{V^I_R}}{dt} \longrightarrow 0 \quad \text{(AIII-10)}$$

because Q/V^I_R is made very large and $\langle \Omega_{Ox.}(r,z,t)\rangle_{V^I_R}$ is finite, then,

$$\langle C_{Ox.}(r,z=L_R,t)\rangle_{A^I_{exit}} - C_{Ox.}(t) \quad \text{(AIII-11)}$$

should be very small but still

$$\frac{dC_{Ox.}(t)}{dt} \qquad \text{(AIII-12)}$$

should be measurable in reasonable time intervals because Q/V_T is also very large.

What is more important, the reactor (V_R^I) will be operating as a differential reactor under pseudo-steady state conditions; then, for the actinometer reaction:

$$\langle \Omega_{Ox.}(r,z,t)\rangle_{V_R^I} = \langle \Omega_{Ox.}(r)\rangle_{V_R^I} \qquad \text{(AIII-13)}$$

at the most.

In fact, as it was said in Appendix AII, under controlled operating conditions the reaction rate is always independent of z in the oxalic acid-uranyl oxalate actinometric reaction (because it is a photosensitized reaction and the uranyl concentration remains constant). However, the above conclusions are extremely important whenever similar conditions apply in the case of the photocatalytic reaction. The final equation results:

$$\frac{d\langle C_{Ox.}(r,z,t)\rangle_{V_{tot.}^I}}{dt} \cong \frac{V_T^I}{V_{tot.}^I}\frac{dC_{Ox.}(t)}{dt} = \frac{V_R^I}{V_{tot.}^I}\langle \Omega_{Ox.}(r)\rangle_{V_R^I} \qquad \text{(AIII-14)}$$

Substituting Eq. (AII-5):

$$\frac{dC_{Ox.}(t)}{dt} = -\frac{V_R^I}{V_T^I}\Phi_\lambda^{Ox.}\langle e_\lambda^a(r)\rangle_{V_R^I} \qquad \text{(AIII-15)}$$

Equation (AIII-15) can be integrated from $t=t_0$ (when $C_{Ox.}(t)=C_{Ox.}^0$) to $t=t$ to give Eq. (16).

Nomenclature

A	area, cm^{-2}; also, optical parameter defined in Table 1, dimensionless
C_i	concentration of the ith component, gmol cm^{-3}
C_m	photocatalyst mass concentration, g cm^{-3}
$\underline{e}$	unit vector with components along the cylindrical coordinates, dimensionless
e_a	local volumetric rate of radiant energy absorption (LVREA), Einstein cm^{-3} s^{-1}
G	incident radiation, Einstein cm^{-2} s^{-1}
I	specific intensity, Einstein cm^{-2} s^{-1} sr^{-1}
j^e	energy emission, Einstein cm^{-3} s^{-1} sr^{-1}
L	length, cm
$\underline{N}$	molar flux, gmol cm^{-2} s^{-1}
$\underline{n}$	unit normal vector, dimensionless
P	lamp output power, W
p	phase function, dimensionless
Q	flow rate, cm^3 s^{-1}
$q^{Rad.}$	radiative flux vector, J cm^{-2} s^{-1}
r	radius, cm; also, radial coordinate, cm
$\underline{r}$	position vector, cm
s	linear coordinate along the direction $\underline{\Omega}$, cm
t	time, s
V	volume, cm^3
v	velocity, cm s^{-1}
z	cylindrical coordinate

Greek letters

α	molar Napierian absorptivity, cm^2 $gmol^{-1}$
β	volumetric extinction coefficient, cm^{-1}
β^*	mass specific extinction coefficient, cm^2 g^{-1}
Δ	parameter defined in Table 1, cm
Φ	quantum yield, gmol $Einstein^{-1}$
η	quantum efficiency, gmol $Einstein^{-1}$
κ	volumetric absorption coefficient, m^{-1}
κ^*	mass specific absorption coefficient, cm^2 g^{-1}
λ	wavelength, nm
ν	frequency, s^{-1}
Θ	defined by Eq. (50), dimensionless
θ	parameter defined in Table 1, cm
σ	volumetric scattering coefficient, cm^{-1}
Ω	solid angle, sr
$\underline{\Omega}$	unit vector in the direction of radiation propagation, dimensionless
Ω_i	reaction rate of component i, gmol cm^{-3} s^{-1}

Subscripts

Chl.	relative to chloroform
R	relative to reactor
1	relative to tube 1
2	relative to tube 2
3	relative to tube 3
P.B.	relative to primary radiation
S.B.	relative to secondary radiation
tot.	relative to total radiation; also, total volume
Ox.	relative to oxalic acid
T	relative to the tank in Fig. 3
w	relative to the reactor wall
Ur.-Ox.	relative to uranyl-oxalate solution
$\underline{\Omega}$	relative to the direction of radiation propagation
ν	indicates a dependence on frequency
λ	indicates a dependence on wavelength

Superscripts

i	relative to an inner radius
e	relative to an external radius
P	relative to the Pyrex glass
R	relative to the infrared filter
$A1$	relative to actinometer in reactor 1
$A2$	relative to actinometer in reactor 2
Ti	relative to titanium suspensions
o	indicates initial conditions
Ox.	relative to oxalic acid

I relative to section I of the experimental device (Fig. 1)

II relative to section II of the experimental device (Fig. 1)

III relative to section III of the experimental device (Fig. 1)

References

[1] D.F. Ollis, E. Pelizzetti and N. Serpone, *Environ. Sci. Technol., 25* (1991) 1523.

[2] L.P. Childs and D.F. Ollis, *J. Catal., 66* (1980) 383.

[3] P. Pichat, J.M. Herrmann, H. Courbon, J. Disdier and M.N. Mozzanega, *Can. J. Chem. Eng., 60* (1982) 27.

[4] M. Schiavello (ed.), *Photoelectrochemistry, Photocatalysis and Photoreactors*, Reidel, Dordrecht, 1985.

[5] E. Pelizetti and N. Serpone (eds.), *Homogeneous and Heterogeneous Photocatalysis*, Reidel, Dordrecht, 1986.

[6] M. Schiavello (ed.), *Photocatalysis and Environment*, Kluwer, Dordrecht, 1988.

[7] R.W. Matthews, *J. Catal., 111* (1988) 264.

[8] R.W. Matthews, *Water Res., 24* (1990) 653.

[9] N. Serpone and E. Pelizetti (eds.), *Photocatalysis: Fundamentals and Applications*, Wiley, New York, 1989.

[10] P. Pichat and J.M. Herrmann, in N. Serpone and E. Pelizetti (eds.), *Photocatalysis Fundamentals and Applications*, Wiley, New York, 1989, p. 217.

[11] E. Pelizetti and M. Schiavello (eds.), *Photochemical Conversion and Storage of Solar Energy*, Kluwer, Dordrecht, 1991.

[12] D.F. Ollis and H. Al-Ekabi (eds.), *Photocatalytic Purification and Treatment of Water and Air*, Elsevier, Amsterdam, 1993.

[13] M. Schiavello, V. Augugliaro and L. Palmisano, *J. Catal., 127* (1991) 332.

[14] V. Augugliaro, L. Palmisano and M. Schiavello, *AIChE J., 37* (1991) 1096.

[15] L. Palmisano, V. Augugliaro, R. Campostrini and M. Schiavello, *J. Catal., 143* (1993) 149.

[16] N. Serpone, R. Terzian, D. Lawless, P. Kennepohl and G. Sauvé, *J. Photochem. Photobiol. A: Chem., 73* (1993) 11.

[17] H.A. Irazoqui, J. Cerdá and A.E. Cassano, *Chem. Eng. J., 11* (1976) 27.

[18] E. Bandini, C. Stramigioli and F. Santarelli, *Chem. Eng. Sci., 32* (1977) 89.

[19] O.M. Alfano, R.L. Romero and A.E. Cassano, *Chem. Eng. Sci., 41* (1986) 421.

[20] G. Spadoni, E. Bandini and F. Santarelli, *Chem. Eng. Sci., 33* (1978) 517.

[21] A.E. Cassano, C.M. Martín, R.J. Brandi and O.M. Alfano, *Ind. Eng. Chem. Res., 34* (1995) 2155.

[22] M.N. Ozisik, *Radiative Transfer and Interactions with Conduction and Convection*, Wiley, New York, 1973.

[23] F. Santarelli, *Lat. Am. J. Heat Mass Transfer, 7* (1983) 35.

[24] M.I. Cabrera, O.M. Alfano and A.E. Cassano, *Ind. Eng. Chem. Res., 33* (1994) 3031.

[25] O.M. Alfano, M.I. Cabrera and A.E. Cassano, *Chem. Eng. Sci., 49* (1994) 5327.

[26] R. Siegel and J.R. Howell, *Thermal Radiation Heat Transfer*, Hemisphere, New York, 1992.

[27] F.C. Baginski, *D. Eng. Dissertation*, Yale University at New Haven, CT, USA, 1951.

[28] E.R. De Bernardez and A.E. Cassano, *Lat. Am. J. Heat Mass Transfer., 6* (1982) 333

[29] A.E. Cassano, O.M. Alfano and R.L. Romero, in S. Whitaker and A.E. Cassano (eds.), *Concepts and Design of Chemical Reactors*, Gordon and Breach, New York, 1986.

[30] R.B. Bird, W.E. Stewart and E.N. Lighfoot, in *Transport Phenomena*, Wiley, New York, 1960.

[31] G. Forbes and L. Heidt, *J. Am. Chem. Soc., 56* (1934) 2363.

[32] D. Volman and J. Seed, *J. Am. Chem. Soc., 86* (1964) 5095.

[33] L. Heidt, G. Tregay and F. Middleton, *J. Phys. Chem., 74* (1970) 1876.

[34] W. Noyes and P. Leighton, in *The Photochemistry of Gases*, Reinhold, New York, 1941.

[35] E.R. De Bernardez and A.E. Cassano, *J. Photochem. Photobiol. A: Chem., 30* (1985) 285.

[36] Canrad Hanovia Inc., *Technical Bulletin: Spectral Energy Distribution of Radiated Mercury Lines in Hanovia-High Pressure Quartz Mercury-Vapor Lamp, Research Laboratory Report: 05/07/76*, 1976.

[37] C.A. Martín, *Doctoral Thesis*, Universidad Nacional del Litoral, Santa Fe, Argentina, 1994.

[38] F.P. Bracket Jr. and G.S. Forbes, *J. Am. Soc., 55* (1933) 4459.

[39] W.G. Leigton and G.S. Forbes, *J. Am. Soc., 52* (1930) 3139.

[40] K. Porter and D.H. Volman, *J. Am. Soc., 84* (1962) 2011.

[41] L.R. Koller, *Ultraviolet Radiation*, Wiley, New York, 1965.

[42] M.A. Clariá, H.A. Irazoqui and A.E. Cassano, *AIChE J., 34* (1988) 366.

[43] C.A. Martín, M.A. Baltanás and A.E. Cassano, *Catal. Today*, 1995, in press.

[44] J.G. Calvert and N.R. Pitts, *Photochemistry*, Wiley, New York, 1966.

[45] A. Braun, M.T. Maurette and E. Oliveros, *Technologie Photochimique*, 1st edn., Presses Polytechniques Romandes, Switzerland, 1986.

[46] C.S. Turchi and D.F. Ollis, *J. Catal., 122* (1990) 178.

[47] D.F. Ollis, in E. Pelizetti and M. Schiavello (eds.), *Photochemical Conversion and Storage of Solar Energy*, Kluwer, Dordrecht, 1991.

[48] R.W. Matthews, in D.F. Ollis and H. Al-Ekabi (eds.), *Photocatalytic Purification and Treatment of Water and Air*, Elsevier, Amsterdam, 1993, p. 121.

[49] C. Kormann, D.W. Bahnemann and M.R. Hoffmann, *Environ. Sci. Technol., 25* (1991) 494.

[50] D.M. Blake, J. Webb, C. Turchi and K. Magrine, *Sol. Energy Mater., 24* (1991) 584.

[51] D. Bahnemann, J. Cunningham, M.A. Fox, E. Pelizetti, P. Pichat and N. Serpone, in G.R. Helz, R.G. Zeep and D.G. Crosby (eds.), *Aquatic and Surface Photochemistry*, Lewis, London, 1994.